

PDF hosted at the Radboud Repository of the Radboud University Nijmegen

The version of the following full text has not yet been defined or was untraceable and may differ from the publisher's version.

For additional information about this publication click this link.

<http://hdl.handle.net/2066/60415>

Please be advised that this information was generated on 2021-09-21 and may be subject to change.

Mott transition and suppression of orbital fluctuations in orthorhombic $3d^1$ perovskites

E. Pavarini,¹ S. Biermann,² A. Poteryaev,³ A. I. Lichtenstein,³ A. Georges,² and O.K. Andersen⁴

¹*INFN and Dipartimento di Fisica "A. Volta", Università di Pavia, Via Bassi 6, I-27100 Pavia, Italy*

²*Centre de Physique Théorique, Ecole Polytechnique, 91128 Palaiseau Cedex, France*

³*NSRIM, University of Nijmegen, NL-6525 ED Nijmegen, The Netherlands*

⁴*Max-Planck-Institut für Festkörperforschung, Heisenbergstrasse 1, D-70569 Stuttgart, Germany*

Using t_{2g} Wannier-functions, a low-energy Hamiltonian is derived for orthorhombic $3d^1$ transition-metal oxides. Electronic correlations are treated with a new implementation of dynamical mean-field theory for non-cubic systems. Good agreement with photoemission data is obtained. The interplay of correlation effects and cation covalency (GdFeO₃-type distortions) is found to suppress orbital fluctuations in LaTiO₃, and even more in YTiO₃, and to favor the transition to the insulating state.

PACS numbers: 71.27.+a, 71.30.+h, 71.15.Ap

Transition-metal perovskites have attracted much interest because of their unusual electronic and magnetic properties arising from narrow $3d$ bands and strong Coulomb correlations [1]. The $3d^1$ perovskites are particularly interesting, since seemingly similar materials have very different electronic properties: SrVO₃ and CaVO₃ are correlated metals with mass-enhancements of respectively 2.7 and 3.6 [2] while LaTiO₃ and YTiO₃ are Mott insulators with gaps of respectively 0.2 and 1 eV [3].

In the Mott-Hubbard picture the metal-insulator transition occurs when the ratio of the on-site Coulomb repulsion and the one-electron bandwidth exceeds a critical value U_c/W , which increases with orbital degeneracy [4, 5]. In the ABO₃ perovskites the transition-metal ions (B) are on a nearly cubic (orthorhombic) lattice and at the centers of corner-sharing O₆ octahedra. The $3d$ band splits into $pd\pi$ -coupled t_{2g} bands and $pd\sigma$ -coupled e_g bands, of which the former lie lower, have less O character, and couple less to the octahedra than the latter. Simplest theories for the d^1 perovskites [1] are therefore based on a Hubbard model with 3 *degenerate*, $\frac{1}{6}$ -filled t_{2g} bands per B-ion, and the variation of the electronic properties along the series is ascribed to a progressive reduction of W due to the increased bending of the $pd\pi$ hopping paths (BOB bonds).

This may not be the full explanation of the Mott transition however, because a splitting of the t_{2g} levels can effectively lower the degeneracy. In the correlated metal, the relevant energy scale is the reduced bandwidth associated with quasiparticle excitations. Close to the transition, this scale is of order $\sim ZW$, with $Z \sim 1 - U/U_c$, and hence much smaller than the original bandwidth W . A level splitting by merely ZW is sufficient to lower the effective degeneracy all the way from three-fold to a non-degenerate single band [6]. This makes the insulating state more favorable by reducing U_c/W [5, 6]. Unlike in e_g -band perovskites, such as LaMnO₃, where large (10%) cooperative Jahn-Teller (JT) distortions of the octahedra indicate that the orbitals are spatially ordered, in the t_{2g} -band perovskites the octahedra are almost perfect. The t_{2g} orbitals have therefore often been assumed to be

generate. If that is true, it is conceivable that quantum fluctuations lead to an orbital *liquid* [7] rather than orbital ordering. An important experimental constraint on the nature of the orbital physics is the observation of an isotropic, small-gap spin-wave spectrum in both insulators [8]. This is remarkable because LaTiO₃ is a G-type antiferromagnet with $T_N=140$ K, $m=0.45 \mu_B$, and a 3% JT stretching along **a** [9], while YTiO₃ is a ferromagnet with $T_C=30$ K, $m_0 \sim 0.8 \mu_B$, and a 3% stretching along **y** on sites 1 and 3, and **x** on 2 and 4 [10] (see Fig. 1).

We shall find that the t_{2g} degeneracy *is lifted* at the classical level. This is not due to the small JT distortions via OB $pd\pi$ -coupling, but to the GdFeO₃-type distortion which tilts the corner-sharing octahedra around the *b*-axis (by 0, 9, 12, and 20°) and rotates them around the *c*-axis (by 0, 7, 9, and 13°), as we progress from cubic SrVO₃ via CaVO₃ and LaTiO₃ to YTiO₃ [9, 10, 11, 12]. This distortion is driven by the increasing oxygen-cation (OA) $pd\sigma$ -covalency, and it primarily pulls closer 4 of the 12 oxygens neighboring a given cation [13]. Moreover, 2 to 4 of the 8 cations neighboring a given B ion are pulled closer [14]. The t_{2g} orbitals couple to the OA distortion via oxygen (BOA $dp\pi$ - $pd\sigma$), and they couple directly (AB $dd\sigma$) to the AB distortion. As seen in Fig. 1, the orthorhombic GdFeO₃-type distortion also leads to quadrupling of the cell. These findings are consistent with conclusions drawn in the most recent model Hartree-Fock study [15]. The correct magnetic orders in LaTiO₃ and YTiO₃ were also obtained with the LDA+ U method [16]. The predicted moment and orbital order in YTiO₃ were confirmed by NMR [17] and neutron scattering [18], but not in LaTiO₃. These static mean-field methods are not appropriate for the metallic systems, however.

In this letter, we shall (i) present a new implementation of a many-body method [19, 20], which allows for a quantitative, material-specific description of *both* the Mott transition and the orbital physics, and (ii) use it to explain why some of the d^1 perovskites are metallic and others are insulators, why the metals have different mass enhancements and the insulators different gaps. Such properties can be described by a low-energy, multi-band

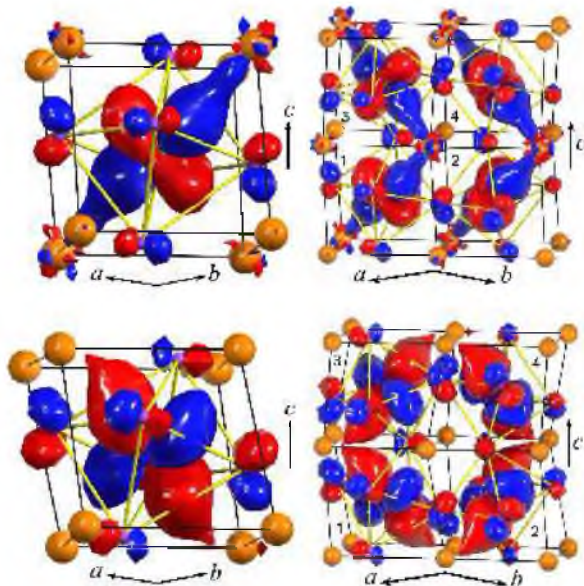


FIG. 1: $Pbnm$ primitive cell (right), subcell1 (left), and the occupied t_{2g} orbitals for LaTiO_3 (top) and YTiO_3 (bottom) according to the LDA+DMFT calculation. The oxygens are violet, the octahedra yellow and the cations orange. In the global, cubic xyz -system directed approximately along the Ti-O bonds, the orthorhombic translations are $\mathbf{a}=(1, -1, 0)(1 + \alpha)$, $\mathbf{b}=(1, 1, 0)(1 + \beta)$, and $\mathbf{c}=(0, 0, 2)(1 + \gamma)$, with α, β, γ small. The Ti sites 1 to 4 are: $\mathbf{a}/2$, $\mathbf{b}/2$, $(\mathbf{a}+\mathbf{c})/2$, and $(\mathbf{b}+\mathbf{c})/2$. The La(Y) ab -plane is a mirror ($z \leftrightarrow -z$), and so is the Ti bc -plane ($x \leftrightarrow y$) when combined with the translation $(\mathbf{b}-\mathbf{a})/2$. See: <http://www.mpi-stuttgart.mpg.de/andersen/cm/0309102.html>

Hubbard Hamiltonian,

$$H = H^{LDA} + \frac{1}{2} \sum_{im m' \sigma} U_{mm'} n_{im\sigma} n_{im'\sigma} + \frac{1}{2} \sum_{im(\neq m')\sigma} (U_{mm'} - J_{mm'}) n_{im\sigma} n_{im'\sigma}, \quad (1)$$

where $n_{im\sigma} = a_{im\sigma}^\dagger a_{im\sigma}$, and $a_{im\sigma}^\dagger$ creates an electron with spin σ in a localized orbital m at site i . This Hamiltonian depends on how the $im\sigma$ -orbitals are chosen. H^{LDA} is the one-electron part given by density-functional theory (LDA), which should provide the proper material dependence. Recently it has become feasible to solve (1) using the *dynamical* mean-field approximation (DMFT) [19] and to obtain realistic physical properties [20]. In the original LDA+DMFT implementations it was assumed that the on-site block(s) of the single-particle Green function is diagonal in the space of the correlated orbitals, and these were taken as orthonormal LMTOs *approximated* by truncated and renormalized partial waves. Although these approximations are good for cubic t_{2g} systems such as SrVO_3 [21], they deteriorate with the degree of distortion. Our new implementation of LDA+DMFT uses a set of localized Wannier functions in order to construct a realistic Hamiltonian (1), which is then solved by DMFT, including the non-

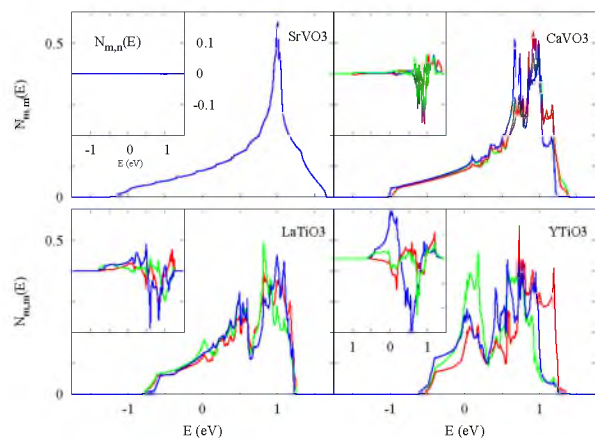


FIG. 2: t_{2g} LDA DOS matrix (states/eV/spin/band) in the Wannier representation. On-site-1 elements: $N_{xz,xx}$ (red) $N_{yz,yz}$ (green), and $N_{xy,xy}$ (blue). Insets: $N_{yz,yz}$ (red), $N_{xz,xy}$ (green), and $N_{xy,yz}$ (blue). $\epsilon_F \equiv 0$.

diagonal part of the on-site self-energy.

For an isolated set of bands, a set of Wannier functions constitutes a *complete*, orthonormal set of orbitals with *one* orbital per band. For the d^1 perovskites we take the correlated orbitals to be three localized t_{2g} Wannier-orbitals, and in H^{LDA} we neglect the degrees of freedom from all other bands. In order to be complete, such a Wannier orbital must have a tail with e.g. $O p\pi$ and $A d$ characters. Our Wannier orbitals are symmetrically orthonormalized N th-order muffin-tin orbitals (NMTOs) [22], which have all partial waves other than Bxy, yz , and zx downfolded. Such a t_{2g} NMTO can have on-site e_g character, and that allows the orbital to orient itself after the surroundings, although xy, yz , and zx refers to the global cubic axes defined in Fig. 1. Fourier transformation of the orthonormalized 12×12 NMTO Hamiltonian, $H^{LDA}(\mathbf{k})$, yields on-site blocks and hopping integrals. For the on-site Coulomb interactions in Eq. (1), we use the common assumption that, as in the isotropic case, they can be expressed in terms of two parameters: $U_{mm}=U$, $U_{mm'}=U - 2J$, and $J_{mm'(\neq m)}=J$ [23]. From Ref. 24, $J=0.68$ eV for the vanadates and 0.64 eV for the titanates. Since our Hamiltonian involves only correlated orbitals, so that the number of correlated electrons is fixed, the double-counting correction amounts to an irrelevant shift of the chemical potential. H is now solved within DMFT, i.e. under the assumption that the components of the self-energy between different sites can be neglected. As a result, the self-energy can be obtained from the solution of an effective local impurity model which involves only 3 correlated orbitals. In contrast to all previous studies, we take all components of the self-energy matrix $\Sigma_{mm'}$ between different Wannier functions on a given B-site into account [25]. From this 3×3 matrix, by use of the $Pbnm$ symmetry (Fig. 1), we con-

struct a 12×12 block-diagonal self-energy matrix. The latter is then used together with $H^{LDA}(\mathbf{k})$ to obtain the Green function at a given \mathbf{k} -point. Fourier transformation over the entire Brillouin zone yields the local Green function associated with a primitive cell and its 3×3 on-site block is used in the DMFT self-consistency condition in the usual manner. The 3-orbital impurity problem is solved by a numerically exact quantum Monte Carlo scheme [26]. To access temperatures down to 770 K, we use up to 100 slices in imaginary time. 10^6 QMC sweeps and 15-20 DMFT iterations suffice to reach convergence. Finally, the spectral function is obtained using the maximum entropy method [27].

We now present the LDA results for the four perovskites. Fig. 2 displays the on-site DOS matrix $N_{mm'}(\varepsilon)$ in the representation of the xy , yz , and zx Wannier functions. SrVO₃ is cubic and its t_{2g} band with a width $W=2.8$ eV consists of 3 non-interacting subbands, each of which is nearly 2D and gives rise to a nearly logarithmic DOS peak. In CaVO₃, W is reduced to 2.4 eV because the Wannier orbitals are misaligned by the GdFeO₃-type distortion and because some of their O $2p$ character is stolen by the increased OA covalency, which drives this distortion. The energy of the xy Wannier orbital (the center of gravity of $N_{xy,xy}$) is 80 meV lower than that of the degenerate xz and yz orbitals, and small off-diagonal DOS elements appear. Going from the vanadates to the titanates, the effects of OA and (A d)(B t_{2g}) covalency increase dramatically, because now A and B are 1st rather than 3rd-nearest neighbors in the periodic table. As consequences, the increased misalignment and loss of oxygen character reduces the bandwidths to 2.1 and 2.0 eV in LaTiO₃ and YTiO₃, and weak hybridization with the A d bands deforms the t_{2g} band. A pseudogap which starts out as a splitting of the van Hove peak in CaVO₃, deepens and moves to lower occupancy as we progress to LaTiO₃ and YTiO₃. The deep pseudogap in YTiO₃ is mainly caused by the hybridization with the Y xy orbital. The xy , yz , and zx Wannier orbitals are now strongly mixed and diagonalization of the on-site blocks of H^{LDA} yields three singly-degenerate levels with the middle (highest) being 140 (200) meV above the lowest in LaTiO₃, and 200 (330) meV in YTiO₃. This splitting is not only an order of magnitude smaller than the t_{2g} bandwidth, but also smaller than the subbandwidths, in particular for LaTiO₃. As a consequence, the eigenfunction for the lowest level is occupied by merely 0.45 electron in LaTiO₃ and 0.50 in YTiO₃, while the remaining 0.55 (0.50) electron occupies the two other eigenfunctions. The eigenfunction on site 1 with the lowest energy is $0.604|xy\rangle + 0.353|xz\rangle + 0.714|yz\rangle$ in LaTiO₃ and $0.619|xy\rangle - 0.073|xz\rangle + 0.782|yz\rangle$ in YTiO₃. The splittings are large compared with the spin-orbit splitting (20 meV) and kT , and they are not caused by the JT distortions, as we have verified by turning them off in the calculations.

Next, we turn to the LDA+DMFT results. Calcula-

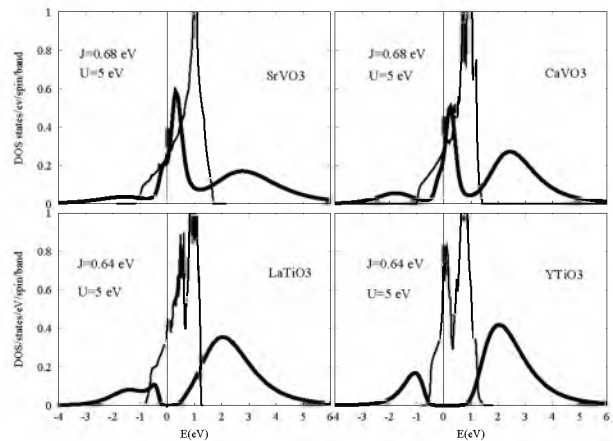


FIG. 3: DMFT spectral function at $T = 770$ K (thick line) and LDA DOS (thin line). $\mu \equiv 0$.

tions were performed for several values of U between 3 and 6 eV. We found that the critical ratio U_c/W decreases when going along the series: SrVO₃, CaVO₃, LaTiO₃, and YTiO₃. This is consistent with the increasing splitting of the t_{2g} levels and indicates that the Mott transition in the d^1 series is driven as much by the decrease of effective degeneracy as by the reduction of bandwidth. The main features of the photoemission spectra for all four materials, as well as the correct values of the Mott-Hubbard gap for the insulators [3], are reproduced by taking U constant ~ 5 eV. This is satisfying, because U is expected to be similar for vanadates and titanates, although slightly smaller for the latter [24]. In Fig. 3 we show the DMFT spectral functions together with the LDA total DOS. For cubic SrVO₃ we reproduce the results of previous calculations [21, 28]: the lower Hubbard band (LHB) is around -1.8 eV and the upper Hubbard band (UHB) around 3 eV. Going to CaVO₃, the quasi-particle peak loses weight to the LHB, which remains at -1.8 eV, while the UHB moves down to 2.5 eV. These results are in good agreement with photoemission data [29] and show that SrVO₃ and CaVO₃ are rather similar, with the latter slightly more correlated. Similar conclusions were drawn in Ref. 21. From the linear regime of the self-energy at small Matsubara frequencies we estimate the quasi-particle weight to be $Z=0.45$ for SrVO₃ and 0.29 for CaVO₃. For a \mathbf{k} -independent self-energy, as assumed in DMFT, this yields $m^*/m = 1/Z = 2.2$ for SrVO₃ and 3.5 for CaVO₃, in reasonable agreement with the optical-conductivity values 2.7 and 3.6 [2].

For LaTiO₃ and YTiO₃ the LHB is around -1.5 eV, in accord with photoemission [30]. Despite very similar bandwidths, the gaps are very different, 0.3 and 1 eV, and this also agrees with experiments [3]. This is consistent with our findings that the t_{2g} -level splittings are smaller and $(U - 2J)_c/W$ is larger in LaTiO₃ than in YTiO₃, where the orbital degeneracy is effec-

tively 1. Diagonalization of the matrix of occupation numbers reveals that for the titanates *one orbital per site is nearly full*, in contrast to LDA. It contains 0.88 electron in LaTiO₃ and 0.96 in YTiO₃. The orbital polarization increases around the metal-insulator transition and becomes complete thereafter. Thus, for the vanadates, each orbital is approximately 1/3 occupied for all U in the range 0 to 6 eV. The *nearly complete* orbital polarization found by LDA+DMFT for the two insulators indicates that correlation effects in the paramagnetic Mott insulating state considerably decrease orbital fluctuations, and makes it unlikely that YTiO₃ is a realization of an orbital liquid [7]. In LaTiO₃ some orbital fluctuations are still active, although quite weak. The occupied orbital in LDA+DMFT is $0.586|xy\rangle + 0.275|xz\rangle + 0.762|yz\rangle$ for LaTiO₃ and $0.622|xy\rangle - 0.029|xz\rangle + 0.782|yz\rangle$ for YTiO₃. Hence, it is nearly identical with the ones we obtained from the LDA as having the lowest energy. For YTiO₃ our orbital is similar to the one obtained in Ref. [16] and for LaTiO₃ it is similar to the one obtained in Refs. [9, 15]. Our accurate Wannier functions show *why* these orbitals (Fig. 1, left) have the lowest energy: The positive (blue) lobes have bonding $3z^2_{111} - 1 = (|xy\rangle + |xz\rangle + |yz\rangle)/\sqrt{3}$ character on the nearest cations –those along [111]– and the negative (red) lobes have bonding xy character on the next-nearest cations –those along [1-11]– whose oxygen surrounding is favorable for this type of bond, i.e. where $(Op)(Yxy)$ p - d -hybridization is strong. The former type of AB covalency dominates in LaTiO₃, while the latter dominates in YTiO₃, where the shortest YO bond is merely 10% longer than the TiO bond. The difference seen (Fig. 1, right side) between the orbital orders in the two compounds is therefore quantitative rather than qualitative; it merely reflects the extent to which the orbital has the bc -plane as mirror. The two different JT distortions of the oxygen square is a reaction to, rather than the cause of the difference in the orbital orders. This difference is reflected in the hopping integrals between nearest neighbors: $t_x=t_y=99$ (38) meV and $t_z=105$ (48) meV for LaTiO₃ (YTiO₃). These hoppings are fairly isotropic and twice larger in LaTiO₃ than in YTiO₃. Moreover, the hoppings to the two excited orbitals are stronger in YTiO₃ than in LaTiO₃. All of this is consistent with LaTiO₃ being G-type anti- and YTiO₃ ferromagnetic at low temperature, and it warrants detailed future calculations of the spin-wave spectra.

In conclusion, we have extended the LDA+DMFT approach to the non-cubic case using ab-initio downfolding in order to obtain a low-energy Wannier Hamiltonian. Applying this method to the Mott transition in $3d^1$ perovskites, we have explained the photoemission spectra and the values of the Mott gap without adjustable parameters, except a single value of U . The Mott transition is driven by correlation effects and GdFeO₃-type distortion through reduction, not only of bandwidth, but also

of effective orbital degeneracy. Correlation effects and cation covalency suppress orbital fluctuations in the high-temperature paramagnetic insulating phase of LaTiO₃ and YTiO₃.

We thank J. Nuss, G. Khaliullin, E. Koch, J. Merino, M. Rozenberg, A. Bringer, M. Imada for useful discussions and the KITP Santa Barbara for hospitality and support (NSF Grant PHY99-07949). Calculations were performed at MPI-FKF Stuttgart and IDRIS Orsay (project No. 021393). S.B. acknowledges support from the CNRS and the EU (Contract No. HPMF-CT-2000-00658).

-
- [1] M. Imada, A. Fujimori, and Y. Tokura, Rev. Mod. Phys. **70**, 1039 (1998).
 - [2] H. Makino *et al.*, Phys. Rev. B **58**, 4384 (1998).
 - [3] Y. Okimoto, *et al.*, Phys. Rev. B **51**, 9581 (1995).
 - [4] M.J. Rozenberg, Phys. Rev. B **55**, R4855 (1997).
 - [5] E. Koch, O.Gunnarsson, R.M. Martin, Phys. Rev. B **60**, 15714 (1999); S. Florens *et al.*, *ibid.* **66**, 205102 (2002).
 - [6] N. Manini, G.E. Santoro, A. Dal Corso, and E. Tosatti, Phys. Rev. B **66**, 115107 (2002).
 - [7] G. Khaliullin, S. Maekawa, Phys. Rev. Lett. **85**, 3950 (2000).
 - [8] B. Keimer *et al.*, Phys. Rev. Lett. **85**, 3946 (2000); C. Ulrich *et al.*, Phys. Rev. Lett. **89**, 167202 (2002).
 - [9] M. Cwik *et al.*, cond-mat/0302087.
 - [10] M. Eitel *et al.*, J. Less-Common Met. **116**, 95 (1986).
 - [11] M.J. Rey *et al.*, J. Solid State Chem. **86**, 101 (1990).
 - [12] M.H. Jung, and H. Nakotte, unpublished.
 - [13] By 0, 10, 13, and 21% of the average OA distance.
 - [14] By 0, 3, 4, and 10% of the average AB distance.
 - [15] M. Mochizuki, and M. Imada, Phys. Rev. Lett. **91**, 167203 (2003); T. Mizokawa, D.I. Khomskii, and G.A. Sawatzky, Phys. Rev. B **60**, 7309 (1999).
 - [16] I. Solovyev, N. Hamada, and K. Terakura, Phys. Rev. B **53**, 7158 (1996); H. Sawada, and K. Terakura, *ibid.* **58**, 6831 (1998).
 - [17] M. Itho *et al.* J. Phys. Soc. Jap. **68**, 2783 (1999).
 - [18] J. Akimitsu *et al.* J. Phys. Soc. Japan **70**, 3475 (2001).
 - [19] A. Georges, G. Kotliar, W. Kraut, M.J. Rozenberg, Rev. Mod. Phys. **68**, 13 (1996).
 - [20] V. Anisimov *et al.* J. J. Phys: Cond. Matt. **9**, 7359 (1997); A. I. Lichtenstein and M. I. Katsnelson, Phys. Rev. B **57**, 6884 (1998).
 - [21] I.A. Nekrasov *et al.*, cond-mat/0211508.
 - [22] O.K. Andersen and T. Saha-Dasgupta, Phys. Rev. B **62**, 16219 (2000); Bull. Mater. Sci. **26**, 19 (2003).
 - [23] R. Fresard and G. Kotliar, Phys. Rev. B **56**, 12909 (1997).
 - [24] T. Mizokawa and A. Fujimori, Phys. Rev. B **54**, 5368 (1996).
 - [25] $\Sigma_{mm'}(\omega) \neq 0$ in non-cubic systems, also in the eigenrepresentation of the density matrix. In Fig. 2, a large $N_{mm'}(\neq m)$ points to a large $\Sigma_{mm'}(\neq m)$.
 - [26] J.E. Hirsch and R.M. Fye, Phys. Rev. Lett. **56**, 2521 (1986).
 - [27] J.E. Gubernatis, M. Jarrell, R. N. Silver and D. S. Sivia, Phys. Rev. B **44**, 6011 (1991).
 - [28] A. Liebsch, Phys. Rev. Lett. **90**, 096401 (2003).
 - [29] K. Maiti *et al.*, Europhys. Lett. **55**, 246 (2001); A. Sekiyama *et al.*, cond-mat/0206471.
 - [30] A. Fujimori *et al.*, Phys. Rev. B **46**, 9841 (1992); K. Morikawa *et al.*, *ibid.* **54**, 8446 (1996).